Nonlocal response in plasmonic waveguiding with extreme light confinement: SUPPLEMENTAL MATERIAL

G. Toscano,[1] S. Raza,[1,2] W. Yan,[1,3] C. Jeppesen,[1] S. Xiao,[1,3]
M. Wubs,[1,3] A.-P. Jauho,[4,3] S. I. Bozhevolnyi,[5] and N. A. Mortensen[1,3*]
[1]*Department of Photonics Engineering, Technical University of Denmark, DK-2800 Kgs. Lyngby, Denmark*
[2]*Center for Electron Nanoscopy, Technical University of Denmark, DK-2800 Kgs. Lyngby, Denmark*
[3]*Center for Nanostructured Graphene (CNG), Technical University of Denmark, DK-2800 Kgs. Lyngby, Denmark*
[4]*Department of Micro and Nanotechnology, Technical University of Denmark, DK-2800 Kgs. Lyngby, Denmark*
[5]*Institute of Technology and Innovation, University of Southern Denmark, DK-5230 Odense, Denmark*

In this supplemental material we offer further details on 1) the derivation of the nonlocal wave equation, 2) the formulation of boundary conditions associated with the hydrodynamic model, 3) the derivation of a generalized energy density expression, and 4) the numerical implementation and its convergence properties.

THE NONLOCAL WAVE EQUATION

In this section of our supplemental material we derive Eq. (2) in our Letter. We start from the coupled hydrodynamic equations, i.e. Eq. (1) in our Letter. Our first step is to isolate $\mathbf{J}$ from Eq. (1a),

$$\mathbf{J} = \frac{1}{i\omega\mu_0}\left\{\nabla\times\nabla\times\mathbf{E} - \left(\tfrac{\omega}{c}\right)^2\varepsilon_\infty\mathbf{E}\right\}, \tag{1}$$

where for generality we have included the ε_∞ interband contribution usually appearing in the Drude permittivity $\varepsilon_D = \varepsilon_\infty - \omega_p^2/[\omega(\omega+i/\tau)]$. Substituting this expression into Eq. (1b) we get

$$\begin{aligned}\tfrac{\beta^2}{\omega(\omega+i/\tau)}\nabla\left[\nabla\cdot\left\{\nabla\times\nabla\times\mathbf{E} - \left(\tfrac{\omega}{c}\right)^2\varepsilon_\infty\mathbf{E}\right\}\right]\\ + \left\{\nabla\times\nabla\times\mathbf{E} - \left(\tfrac{\omega}{c}\right)^2\varepsilon_\infty\mathbf{E}\right\} = i\omega\mu_0\sigma\mathbf{E}.\end{aligned} \tag{2}$$

Next, for any vector field $\mathbf{F}$, the divergence of its curl is zero, i.e. $\nabla\cdot(\nabla\times\mathbf{F}) = 0$. Thus, without loss of generality the expression now simplifies to

$$\begin{aligned}-\tfrac{\beta^2}{\omega(\omega+i/\tau)}\left(\tfrac{\omega}{c}\right)^2\varepsilon_\infty\nabla\left[\nabla\cdot\mathbf{E}\right]\\ + \left\{\nabla\times\nabla\times\mathbf{E} - \left(\tfrac{\omega}{c}\right)^2\varepsilon_\infty\mathbf{E}\right\} = i\omega\mu_0\sigma\mathbf{E}.\end{aligned} \tag{3}$$

Furthermore, utilizing that in general $\nabla\left[\nabla\cdot\mathbf{F}\right] = \nabla\times\nabla\times\mathbf{F} + \nabla^2\mathbf{F}$ we get

$$\begin{aligned}-\tfrac{\beta^2}{\omega(\omega+i/\tau)}\left(\tfrac{\omega}{c}\right)^2\varepsilon_\infty\left\{\nabla\times\nabla\times\mathbf{E} + \nabla^2\mathbf{E}\right\}\\ + \left\{\nabla\times\nabla\times\mathbf{E} - \left(\tfrac{\omega}{c}\right)^2\varepsilon_\infty\mathbf{E}\right\} = i\omega\mu_0\sigma\mathbf{E}.\end{aligned} \tag{4}$$

Re-grouping the double-curl terms on the left-hand side (as in the common LRA wave equation) and re-introducing the local-response Drude permittivity as $\varepsilon_D = \varepsilon_\infty + i\sigma/(\varepsilon_0\omega)$ we get

$$\nabla\times\nabla\times\mathbf{E} = \left(\tfrac{\omega}{c}\right)^2\mathcal{K}\left[\varepsilon_D + \tfrac{\beta^2\varepsilon_\infty}{\omega(\omega+i/\tau)}\nabla^2\right]\mathbf{E}. \tag{5}$$

For the re-normalization on the right-hand side we note that $\mathcal{K} = \frac{c^2}{c^2-\beta^2\varepsilon_\infty(1+i/\omega\tau)^{-1}} = 1 + \mathcal{O}(\varepsilon_\infty[\beta/c]^2[1 - i/\omega\tau]^{-1})$ and for all practical purposes involving the common noble metals it is close to unity. In this way we end up with Eq. (2) in our Letter.

TRANSLATIONALLY INVARIANT SYSTEMS

For infinite systems with translational invariance it is convenient to work in Fourier space and this has been the common approach in most of the early literature. To connect our result in Eq. (5) to $\mathbf{k}$-space formalism we Fourier transform the wave equation which gives

$$-\mathbf{k}\times\mathbf{k}\times\mathbf{E} = \left(\tfrac{\omega}{c}\right)^2\left(1 - \tfrac{\omega_p^2}{\omega^2}\right)\mathbf{E} - \left(\tfrac{\beta}{c}\right)^2\mathbf{k}\left(\mathbf{k}\cdot\mathbf{E}\right), \tag{6}$$

where for simplicity we have suppressed the interband contribution and the damping. Below, we will use the Helmholtz decomposition $\mathbf{E} = \mathbf{E}_t + \mathbf{E}_l$ and to clearly distinguish between transverse fields ($\mathbf{k}\cdot\mathbf{E}_t = 0$) and longitudinal fields ($\mathbf{k}\times\mathbf{E}_l = 0$) we have above in the Laplacian term deliberately used the identity given below Eq. (3).

For longitudinal fields we now get

$$0 = \left(\omega^2 - \omega_p^2 - \beta^2 k_l^2\right)\mathbf{E}_l, \tag{7a}$$

or alternatively, pulling a factor $(\omega^2 - \beta^2 k_l^2)$ outside the parenthesis, we get

$$0 = \left(1 - \tfrac{\omega_p^2}{\omega^2 - \beta^2 k_l^2}\right)\mathbf{E}_l. \tag{7b}$$

Thus, we immediately find that the non-trivial longitudinal solutions have dispersion relation $\omega(k_l) = \sqrt{\omega_p^2 + \beta^2 k_l^2}$, i.e. we exactly recover the classical solution for longitudinal bulk plasmons commonly derived from $\varepsilon_l(\omega, k_l) \equiv 0$ where $\varepsilon_l(\omega, k_l) = 1 - \omega_p^2/(\omega^2 - \beta^2 k_l^2)$.

Likewise, for transverse fields we get

$$k_t^2\mathbf{E}_t = \left(\tfrac{\omega}{c}\right)^2\left(1 - \tfrac{\omega_p^2}{\omega^2}\right)\mathbf{E}_t, \tag{8}$$

so that we arrive at the common transverse dispersion relation $k_t = (\omega/c)\sqrt{\epsilon_t(\omega)}$ where $\varepsilon_t(\omega) = \varepsilon_l(\omega, k \to 0) = 1 - \omega_p^2/\omega^2$.

BOUNDARY CONDITIONS

The Eq. (2) in our Letter must be equipped with a physically appropriate boundary condition, as we discussed in Ref. [1] and more recently in detail in an appendix of Ref. [2]. This condition can be easily worked out from the continuity of the normal component of the displacement vector $\mathbf{D}$ across the boundaries, that reads:

$$\mathbf{D}_m \cdot \hat{\mathbf{n}} = \mathbf{D}_d \cdot \hat{\mathbf{n}} \tag{9}$$

where m indicates the metal and d refers to the surrounding dielectric material. The displacement vector in the metal is defined as:

$$\mathbf{D}_m = \varepsilon_0 \varepsilon_\infty \mathbf{E} + \frac{i}{\omega}\mathbf{J}, \tag{10}$$

where $\mathbf{J}$ is the free-electron current density. The displacement vector in the dielectric material reads:

$$\mathbf{D}_m = \varepsilon_0 \varepsilon_d \mathbf{E}, \tag{11}$$

where ε_d is the permittivity of the surrounding material.

Equation (9) can now be rewritten as:

$$\left(\varepsilon_0 \varepsilon_\infty \mathbf{E}_m + \frac{i}{\omega}\mathbf{J}\right) \cdot \hat{\mathbf{n}} = \varepsilon_0 \varepsilon_d \mathbf{E}_d \cdot \hat{\mathbf{n}} \tag{12}$$

Next, we impose the boundary condition $\mathbf{J} \cdot \hat{\mathbf{n}} = 0$, discussed in detail in Refs. [1, 2], which gives

$$\varepsilon_\infty \mathbf{E}_m \cdot \hat{\mathbf{n}} = \varepsilon_d \mathbf{E}_d \cdot \hat{\mathbf{n}}. \tag{13}$$

This equation states that the normal component of the electric field is continuous across the boundaries only when interband contributions are neglected and the surrounding material is free space. Eq. (2) in our Letter is solved subject to this boundary condition. We emphasize that this is fully consistent with original requirement that $\mathbf{J} \cdot \hat{\mathbf{n}} = 0$ on the boundary.

GENERALIZED ENERGY DENSITY

In this section of our supplemental material we derive a generalized expression for the electromagnetic energy density, including the contributions stored in the hydrodynamics of the free-electron gas. We start from the Poynting theorem in time domain [3]

$$\int_S \mathbf{E}\times\mathbf{H}\cdot\,\hat{\mathbf{n}}\,d\mathbf{S} = -\int_V \left[\varepsilon_0 \mathbf{E}\cdot\dot{\mathbf{E}} + \mathbf{E}\cdot\dot{\mathbf{P}} + \mu_0 \mathbf{H}\cdot\dot{\mathbf{H}}\right] dV \tag{14}$$

where $\mathbf{P}$ is the polarization vector, V is the volume of the electron gas, and S is its boundary. The polarization current $\mathbf{J}$ is linked to $\mathbf{P}$ by

$$\mathbf{J} = \frac{\partial \mathbf{P}}{\partial t} = \dot{\mathbf{P}}. \tag{15}$$

At the same time, the polarization current is related to the electric field by means of the hydrodynamic equation. In time domain, the linearized hydrodynamic Euler equation for the electron dynamics is

$$m_e \frac{\partial \mathbf{v}}{\partial t} = -\beta^2 \frac{m_e}{n_o}\nabla n - m_e \gamma \mathbf{v} - e\mathbf{E} \tag{16}$$

where $\mathbf{v}$ is the electron velocity, n is the electron density, n_0 is the electron density at rest, and m_e the electron mass. If we introduce the polarization current $\mathbf{J} = -en_0\mathbf{v}$ and the charge density $\rho = -en$, the Eq. (16) becomes

$$\frac{\partial \mathbf{J}}{\partial t} = -\beta^2 \nabla\rho - \gamma \mathbf{J} + \varepsilon_0 \omega_p^2 \mathbf{E}. \tag{17}$$

Next, if we use the definition (15), and the continuity equation $\rho = -\nabla \cdot \mathbf{P}$, we get

$$\beta^2 \nabla\nabla \cdot \mathbf{P} - \frac{\partial^2 \mathbf{P}}{\partial t^2} - \gamma \frac{\partial \mathbf{P}}{\partial t} + \varepsilon_0 \omega_p^2 \mathbf{E} = 0. \tag{18}$$

We can now isolate $\mathbf{E}$ in this expression,

$$\mathbf{E} = -\frac{1}{\varepsilon_0 \omega_p^2}\left[\beta^2 \nabla\nabla \cdot \mathbf{P} - \frac{\partial^2 \mathbf{P}}{\partial t^2} - \gamma \frac{\partial \mathbf{P}}{\partial t}\right] \tag{19}$$

and multiplying by $\dot{\mathbf{P}}$, we get

$$\mathbf{E} \cdot \dot{\mathbf{P}} = -\frac{1}{\varepsilon_0 \omega_p^2}\left[\beta^2 \nabla\nabla \cdot \mathbf{P} \cdot \dot{\mathbf{P}} - \frac{1}{2}\frac{d\dot{\mathbf{P}}^2}{dt} - \gamma \dot{\mathbf{P}}^2\right]. \tag{20}$$

In the spirit of Eq. (14) we now integrate Eq. (20) over the metallic volume,

$$\int_V \mathbf{E}\cdot\dot{\mathbf{P}}\,dV = -\frac{1}{\varepsilon_0 \omega_p^2}\int_V \left[\beta^2 \nabla\nabla\cdot\mathbf{P}\cdot\dot{\mathbf{P}} - \frac{1}{2}\frac{d\dot{\mathbf{P}}^2}{dt} - \gamma\dot{\mathbf{P}}^2\right] dV. \tag{21}$$

Our next step is to integrate by part,

$$\int_V \nabla\nabla\cdot\mathbf{P}\cdot\dot{\mathbf{P}}\,dV = -\int_V \nabla\cdot\mathbf{P}\,\nabla\cdot\dot{\mathbf{P}}\,dV + \int_S \nabla\cdot\mathbf{P}\,\dot{\mathbf{P}}\cdot\hat{\mathbf{n}}\,d\mathbf{S}$$

To further proceed, we now apply the physical boundary condition $\mathbf{J}\cdot\hat{\mathbf{n}} = 0$ [1], i.e. no electrons leaving the metal volume. This gives

$$\int_V \nabla\nabla\cdot\mathbf{P}\cdot\dot{\mathbf{P}}\,dV = -\int_V \frac{1}{2}\frac{d(\nabla\cdot\mathbf{P})^2}{dt}\,dV.$$

In this way Eq. (21) now reads

$$\int_V \mathbf{E}\cdot\dot{\mathbf{P}}\,dV = \frac{1}{\varepsilon_0\omega_p^2}\int_V \left[\frac{\beta^2}{2}\frac{d(\nabla\cdot\mathbf{P})^2}{dt} + \frac{1}{2}\frac{d\dot{\mathbf{P}}^2}{dt} + \gamma\dot{\mathbf{P}}^2\right] dV \tag{22}$$

and substituting into the Poynting theorem, Eq. (14), we get

$$\int_S \mathbf{E}\times\mathbf{H}\cdot\,\hat{\mathbf{n}}\,d\mathbf{S}+\int_V \frac{\gamma}{\varepsilon_0\omega_p^2}\dot{\mathbf{P}}^2\,dV=-\int_V \dot{u}\,dV. \quad (23)$$

Here, u is the electromagnetic energy density defined as

$$u=\frac{1}{2}\varepsilon_0\mathbf{E}^2+\frac{\beta^2}{2\varepsilon_0\omega_p^2}\left(\nabla\cdot\mathbf{P}\right)^2+\frac{1}{2\varepsilon_0\omega_p^2}\dot{\mathbf{P}}^2+\frac{1}{2}\mu_0\mathbf{H}^2. \quad (24)$$

Finally, if we recall the continuity equation for the polarization charge density, given by $\rho=-\nabla\cdot\mathbf{P}$, and we use Eq. (15), then

$$u=\frac{1}{2}\varepsilon_0\mathbf{E}^2+\frac{\beta^2}{2\varepsilon_0\omega_p^2}\rho^2+\frac{1}{2\varepsilon_0\omega_p^2}\mathbf{J}^2+\frac{1}{2}\mu_0\mathbf{H}^2. \quad (25)$$

This is our generalization of the common energy-density to account for the energy stored in the additional degrees of freedom associated with the nonlocal hydrodynamics of the electron gas. For time harmonic fields, this expression can easily be time-averaged.

In our Letter, we focus on electrical dipole emitters where the $\mathbf{H}$ contribution can be neglected. For our accurate numerical evaluation we rely on Eqs. (1) in our Letter, i.e. an eigenvalue-problem with a six-element eigenvector $\{\mathbf{E},\mathbf{J}\}$, rather than Eqs. (2) where one would in a subsequent (and less accurate) step have to numerically derive $\mathbf{J}$ from the obtained 3-element eigenvector $\{\mathbf{E}\}$.

NUMERICAL IMPLEMENTATION AND CONVERGENCE

In this section of our supplemental material we offer some details on the numerical implementation and the convergence tests for the waveguides that we have analyzed in our Letter. For scattering problems involving arbitrarily shaped metal geometries, Eq. (1) can be solved numerically with the aid of finite-element methods [4]. In particular, the hydrodynamic model can conveniently be integrated into commercially available software such as Comsol Multiphysics. For the scattering problem we have already made such an add-on to Comsol Multiphysics freely available [5]. Here, we extend this approach to an eigenvalue problem appropriate for waveguiding problems. Our code for solving Eq. (2) in our Letter is an add-on to Comsol Multiphysics 4.1, employing the PDE Weak form module and the standard MUMPS eigenvalue solver.

For our discussion of the numerical convergence we first note that in Fig. 2 of our Letter, the agreement between the analytical and numerical solutions is very good. More quantitatively, the relative error of the numerically calculated propagation constant k_z with respect to the analytical value is always smaller than 0.3% in the entire frequency range of Fig. 2. Likewise, the relative error for the effective mode area $A_{\rm eff}$ is always smaller than 0.12% within the same frequency range.

The convergence analysis for the circular nanowire waveguides is based on the methodology that we have described in previous work for the scattering problem [4]. In the present case we have two observables, i.e. the propagation constant k_z and the effective mode area $A_{\rm eff}$. Thus, we define the relative errors $\delta_k^{\rm num}$ and $\delta_A^{\rm num}$ according to the definition $\delta_x^{\rm num}=\left|x_{\rm mesh}-x_{\rm reg}\right|/x_{\rm reg}$ where $x_{\rm mesh}$ is the observable value at fixed mesh edge number and $x_{\rm reg}$ is the value in the convergence regime. To illustrate the convergence performance we consider a relatively high frequency $\omega=0.6\omega_p$, because in this case the field is mainly localized in the metal. This represents a "worst-case" condition for the calculations because a high number of edge elements is needed. The results are shown in Fig. S1 for a varying number η of triangular elements while we for late convenience introduce $\bar{\eta}$ as the normalized number of triangular elements. It is important to underline that the propagation constant k_z is calculated by means of the Eq. (2) in our Letter, while the mode area is calculated with Eq. (1) of our Letter, i.e. providing us with both the electrical field and the current density. As clearly seen, both codes show a convergence of the calculated parameters for $\eta>250$. The corresponding simulation time is about 5 min for both codes. The faster convergence of Eq. (2) over Eq. (1) is also noted when comparing panels (a) and (b).

The convergence test for the V-groove is performed for the case $\lambda=600\,$nm, because it corresponds to the maximum field localization in the visible spectrum, and a high mesh density is needed. The observables are the effective refractive index $n_{\rm eff}$ and the propagation length L. As seen in Fig. S2, both relative errors $\delta_{\rm n}^{\rm num}$ and $\delta_{\rm L}^{\rm num}$ converge for $\bar{\eta}>200$, and the simulation time is about 10 min. These dispersion results were calculated from Eq. (2) in our Letter.

The convergence test for the Λ-wedge structure follows the same lines. Also in this case, we show the test performed at $\lambda=600\,$nm, that corresponds to the highest field confinement in the metal. The results are shown in Fig. S3 and we notice that the propagation length converges at higher η with respect to the effective refractive index. The Λ-wedge presents high losses at this wavelength, and the simulations can be very sensitive on the mesh density. The results are obtained from Eq. (2) in our Letter, and the typical computation time is about 10 min.

Finally, we consider the convergence of the effective mode area for both V-groove and Λ-wedge. The results are shown in Fig. S4. Note that the mesh densities in the two cases are relative to different geometrical entities, so they cannot be compared directly. The results for the mode area are calculated with Eq. (1) of our Letter, i.e. providing us with both the electrical field and the current

density. The simulation time is about 10 min also in this case.

* Electronic address: asger@mailaps.org

[1] S. Raza, G. Toscano, A.-P. Jauho, M. Wubs, and N.A. Mortensen, Phys. Rev. B **84**, 121412(R) (2011).
[2] W. Yan, M. Wubs, and N.A. Mortensen, Phys. Rev. B **86**, 205429 (2012).
[3] R. Ruppin, Phys. Lett. A **299**, 309-312 (2002).
[4] G. Toscano, S. Raza, A.-P. Jauho, N. A. Mortensen, and M. Wubs, Opt. Express **20**, 4176 (2012).
[5] www.nanopl.org

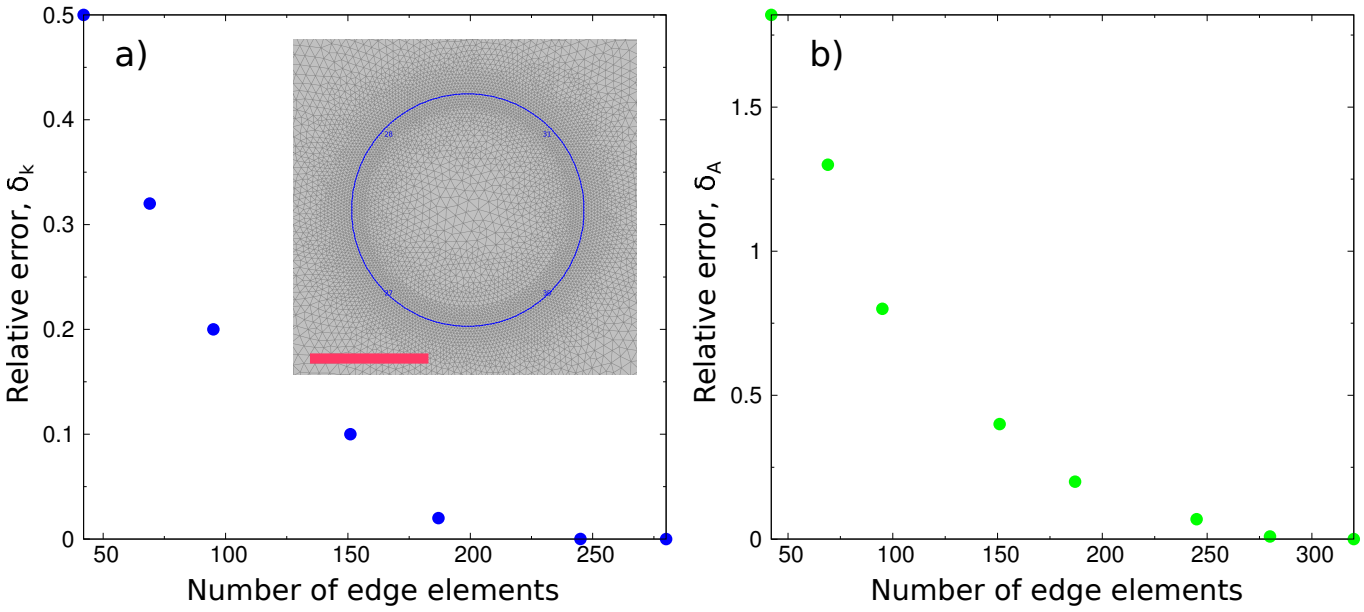

FIG. 1: Convergence test for a cylindrical nanowire with radius $R = 2$ nm. Panel a) Relative error $\delta_k^{\rm num}$ of the propagation constant k_z versus number of edge elements for cylindrical nanowires. The convergence occurs for $\eta > 200$. Panel b) Relative error $\delta_A^{\rm num}$ of the effective mode area $A_{\rm eff}$ versus number of edge elements for cylindrical nanowires. The convergence occurs for $\eta > 250$. The scale bar is 1 nm long. The inset refers to $\eta = 250$.

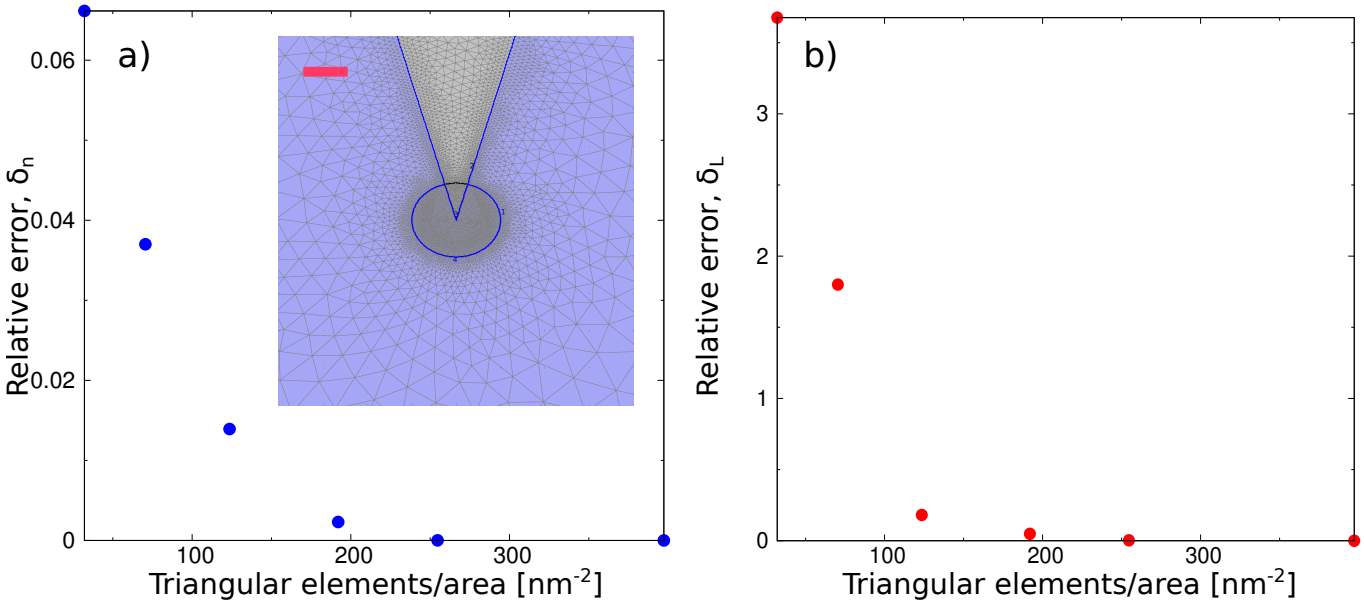

FIG. 2: Convergence test for a V-groove structure with aperture angle $\theta = 30^\circ$. The radius of the meshing circle $R_{\rm mesh} = 10$ nm, and it is kept constant while varying the number of triangular elements. Panel a) Relative error $\delta_n^{\rm num}$ of the effective refractive index versus the normalized number of triangular elements $\bar{\eta}$. The convergence occurs for $\bar{\eta} > 200$, that corresponds to 6283 elements. Panel b) Relative error $\delta_L^{\rm num}$ of the propagation length L versus $\bar{\eta}$. The convergence occurs for $\bar{\eta} > 200$. The scale bar is 10 nm long. The inset refers to $\bar{\eta} = 200$, and the shaded blue area indicates the metal.

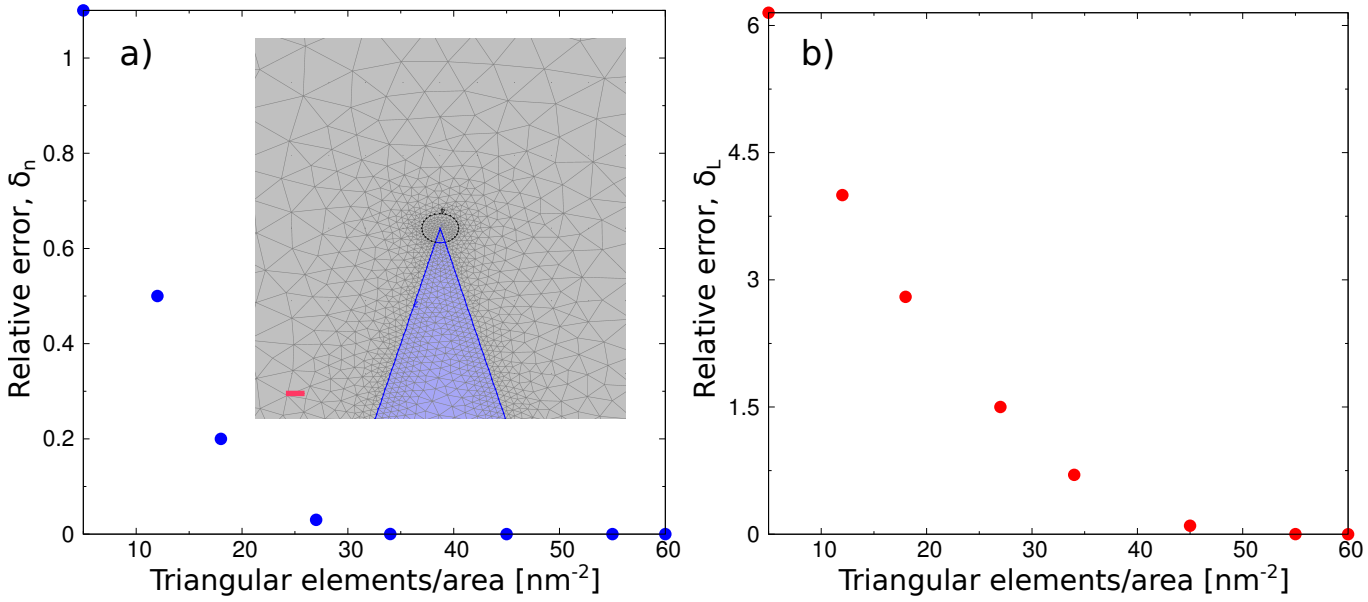

FIG. 3: Convergence test for a Λ-wedge structure with aperture angle $\theta = 30^\circ$. The radius of the meshing circle $R_{\rm mesh} = 1\,$nm, and it varies, while the number of triangular elements is kept constant. Panel a) Relative error $\delta_n^{\rm num}$ of the effective refractive index versus the normalized number of triangular elements η. The convergence occurs for $\bar{\eta} > 30$, that corresponds to $\eta > 94$ elements. Panel b) Relative error $\delta_L^{\rm num}$ of the propagation length L versus $\bar{\eta}$. The convergence occurs for $\bar{\eta} > 45$, i.e. $\eta > 141$. The scale bar is 1 nm long. The inset refers to $\bar{\eta} = 141$, and the shaded blue area indicates the metal.

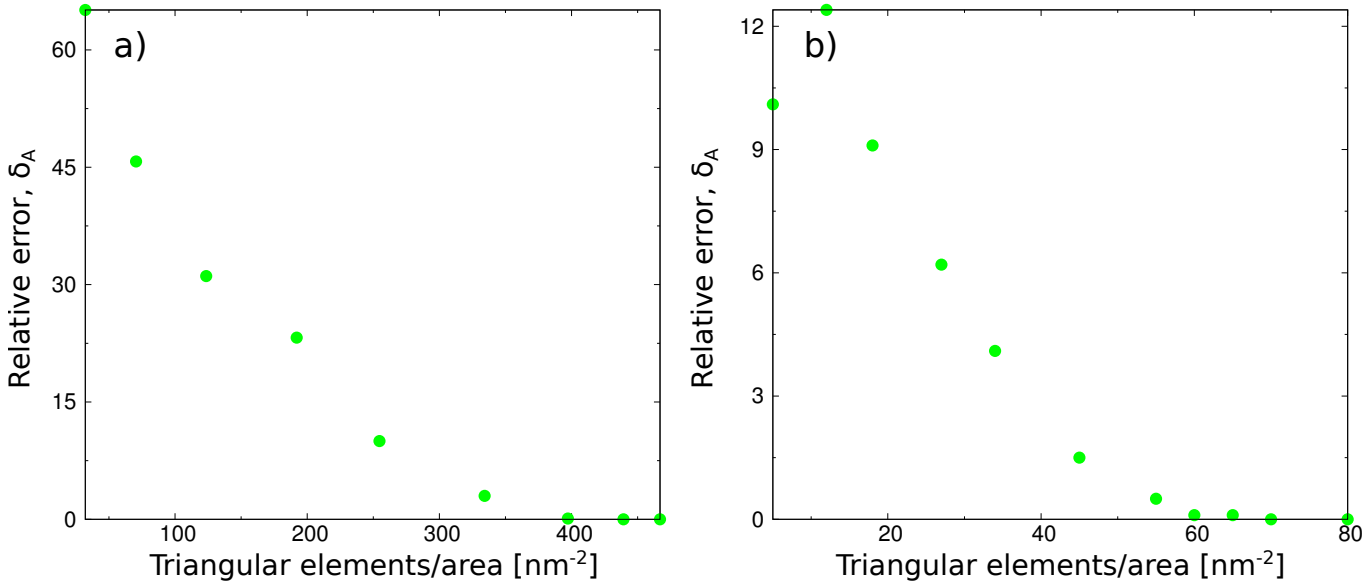

FIG. 4: Convergence test for the effective mode area for V-groove and Λ-wedge waveguides. Panel a) Relative error $\delta_A^{\rm num}$ of the effective mode area $A_{\rm eff}$ versus number of edge element for the V-groove. The convergence occurs for $\bar{\eta} > 400$, i.e. $\eta > 12566$. Panel b) Relative error $\delta_A^{\rm num}$ of the effective mode area $A_{\rm eff}$ versus number of edge elements for the Λ-wedge waveguide. The convergence occurs for $\bar{\eta} > 60$, i.e. $\eta > 188$.